Journal of Inorganic and Organometallic Polymers and Materials (2020) 30:1695–1702
https://doi.org/10.1007/s10904-019-01337-3

A Magnetic Plasmonic Catalyst Based on Monodisperse-Porous Silica Microspheres for Rapid Reduction of 4-Nitrophenol

Çiğdem Kip[1]

Received: 8 July 2019 / Accepted: 25 September 2019 / Published online: 28 September 2019

Abstract
In this work, the degradation of 4-nitrophenol (4-NP) was investigated by using plasmonic gold nanoparticles decorated magnetic-porous silica microspheres (AuNP@Mag–SiO_2) as catalyst in the presence of excess sodium borohydride ($NaBH_4$) in batch fashion. Magnetic silica microspheres (Mag–SiO_2), 6.20 µm in size synthesized with high surface area and good magnetic properties were functionalized with amine groups. Using these particles as support, immobilization of gold nanoparticles (AuNP) was performed. The morphological, chemical and magnetic properties of the catalyst were analyzed by Scanning electron microscopy (SEM), Surface area and pore size analyzer, X-ray diffraction spectroscopy (XRD), Vibrating sample magnetometer (VSM) and X-ray photoelectron spectroscopy (XPS). The plasmonic catalytic activities of AuNP@Mag–SiO_2 microparticles were investigated by the reduction of 4-nitrophenol (4-NP) to 4-aminophenol (4-AP) monitored by UV–Vis spectroscopy by changing the reaction parameters such as amount of catalyst, Au loading, initial 4-NP concentration, and reaction temperature. Reaction times ranging between 5 and 30 min were obtained in the quantitative reduction of 4-NP using gold nanoparticles decorated magnetic silica (AuNP@Mag–SiO_2) microspheres. The plasmonic catalyst was recovered efficiently by magnetic separation and highly stable without exhibiting no significant activity decrease with the repeated use.

Keywords Sol–gel template · Plasmonic catalysis · 4-Nitrophenol · Magnetic silica microspheres

1 Introduction

The rapid developments in nanotechnology have led to products developed to gain an important place in many fields such as imaging, biosensing, photothermal therapy and catalysts [1–15]. There has been a growing interest in the use of gold nanoparticles (AuNP) as catalysts due to their high plasmonic catalytic activity, better selectivity, unique and tunable optical properties and longer stability properties [16–22].

In general, nanoparticles in solution tend to aggregate due to their high surface energies, which leads to a significant reduction in catalytic activity [23, 24]. Although gold nanoparticles show plasmonic catalytic activity, they tend to agglomerate in the reaction medium [25]. In order to increase the catalyst stability, AuNP can be immobilized to different support materials (such as carbon nanotubes, silica, titanium) [26–29]. Among them, porous silica microspheres are preferred because of their good compatibility, chemical and thermal stability. In particular, the mesoporous of compartment of silica based materials provides high surface area and large pore volume that can increase the active sites of the catalysts, while the macroporous compartment provides efficient mass transfer [30–32]. Due to its inert structure, silica also gives high catalytic activity by reducing the metal-support interaction. To increase the amount of nanoparticles on the surface of the support material, the support material surface can be functionalized with groups such as $–NH_2$ [33, 34]. However, the isolation of the catalysts from the reaction medium (centrifugation or filtration) is a time-consuming and difficult process. Magnetic particles are used to overcome this problem. For facile recyclability, magnetic catalysts can be rapidly separated from the reaction mixture by applying an external magnet [35–37].

Electronic supplementary material The online version of this article (https://doi.org/10.1007/s10904-019-01337-3) contains supplementary material, which is available to authorized users.

✉ Çiğdem Kip
cigdemg@hacettepe.edu.tr

[1] Chemical Engineering Department, Hacettepe University, Ankara, Turkey

The reduction of 4-NP to 4-aminophenol by $NaBH_4$ which have been widely used as a model reaction in the investigation of the catalytic properties of different nanoparticles, were first reported in 2002 [38–43]. 4-aminophenol is an important intermediate in the preparation of antipyretic drugs such as acetaminophen and various painkillers such as acetanilide and phenacetin. It is also used as corrosion inhibitor in paints and fuels. It is important to develop a cheap and efficient catalyst for catalytic reduction of 4-NP in aqueous solution under mild conditions. Hence, the removal of 4-nitrophenol from the contaminated samples is particularly important for reducing the pollution in aquatic media. Pt nanoparticles carrying bimetallic supported catalysts were efficiently used for reduction of 4-nitrophenol to 4-aminophenol [44–46]. Au/m–SiO_2/Fe_3O_4 catalyst was developed for the catalytic reduction of p-nitrophenol with $NaBH_4$ by Liu et al. [47]. In other work, the reduction of nitroaromatic compounds was examined by using Fe_3O_4@SiO_2–Au@mSiO_2 in the presence of sodium borohydride [41]. Li et al. reported that Au@Fe_3O_4/*m*–SiO_2 yolk@shell nanocatalysts showed high catalytic activity with high stability and recyclability due to the synergetic effect of Au and Fe_3O_4 interactions [48]. Wang et al. prepared Au@SiO_2 nanocatalyst by a typical Stober method and the catalytic performances of nanocatalyst was investigated in 4-nitrophenol reduction [49]. Deng et al. proposed Fe_3O_4@SiO_2–Au@mSiO_2 microspheres as catalyst with high activity for the catalytic reduction of 4-nitrophenol in room temperature [40]. Dong et al. prepared AuNP decorated magnetic fibrous silica microspheres and investigate their catalytic activity in the reduction of 4-NP [50]. In another study, AuNP were grafted on the amine or thiol functionalized magnetic silica nanoparticles and their catalytic activities were tested in the catalytic reduction of 4-NP with $NaBH_4$ [36]. Zhang et al. reported the synthesis of Au-decorated silica spheres as a catalyst for use in the reduction reaction [51]. Zhou et al. evaluated the catalytic activity of gold catalyst immobilized on ordered arrays of multilamellar silica nanoparticles in reduction of 4-NP [52].

In this work, the catalytic activity of gold nanoparticles decorated magnetic, monodisperse-porous silica (AuNP@Mag–SiO_2) microspheres were proposed as a catalyst with high activity, magnetic separability and good reusability for the reduction of 4-NP in batch fashion. The effects of amount of catalyst, Au loading, initial concentration of 4-NP and reaction temperature on the catalytic activity were investigated in the presence of excess amount of $NaBH_4$ in the reaction medium.

2 Experimental Section

2.1 Chemicals and Materials

For the synthesis of monodisperse-porous poly(methacrylic acid-co-ethylene glycol dimethacrylate [poly(MAA-co-EDMA)] microspheres; the monomers, glycidyl methacrylate (GMA), methacrylic acid (MAA), the crosslinking agent, ethylene dimethacrylate (EDMA) and the diluent, ethylbenzene (EB) were supplied from Aldrich Chem. Corp., USA. The initiator, benzoyl peroxide (BPO), the stabilizer, polyvinyl alcohol (PVA, 87–89% hydrolyzed, Mw = 85,000–146,000) and polyvinylpyrrollidone (PVP K-30, Sigma, average molecular weight: 40,000 Da), the emulsifier, sodium dodecyl sulfate (SDS) were supplied from Aldrich. The initiator, BPO was dried under vacuum at 30 °C before use. 2,2-azobisisobutyronitrile (AIBN) supplied from Across Organics, USA were recrystallized from methanol before use. Ethanol (EtOH, HPLC grade, Merck A.G., Darmstadt, Germany), isopropanol (Iso-PrOH, HPLC grade, Aldrich) and tetrahydrofuran (THF, HPLC grade, Aldrich) were used as the solvents. Tetraethyl orthosilicate (TEOS) as precursor, tetrabutylammonium iodide (TBAI) and ammonium hydroxide solution (NH_4OH, 26% w/w) were also purchased from Sigma. Distilled deionized (DDI) water (Direct-Q 3 UV (Type 1), Millipore, USA) with a resistivity of 18 MΩ cm was used during all synthesis runs. For the magnetization of poly (MAA-co-EDMA) microspheres, iron(III) chloride hexahydrate ($FeCl_3{\cdot}6H_2O$) and iron(II) chloride tetrahydrate ($FeCl_2{\cdot}4H_2O$) were obtained from Sigma-Aldrich Co, USA. For the derivatization of magnetic silica microspheres with amine groups, aminopropyltriethoxysilane (APTES, Sigma Chemical Co., St. Louis, MO, USA) and triethylamine (TEA, Sigma Chemical Co., St. Louis, MO, USA) were used. For the synthesis of gold nanoparticles, chloroauric acid trihydrate ($HAuCl_4{\cdot}3H_2O$, Sigma Chemical Co., St. Louis, Mo., USA), trisodium citrate (TSS, Sigma Chemical Co., St. Louis, Mo., USA), sodium borohydride ($NaBH_4$, Sigma Chemical Co., St. Louis, MO, USA) were used. Sodium hydroxide (NaOH, Sigma Chemical Co., St. Louis, Mo., USA) and hydrochloric acid (HCl, 37% w/w, Sigma Chemical Co., St. Louis, Mo., USA) were used to prepare $NaBH_4$ and $HAuCl_4$ solutions, respectively. In order to determine the degradation of 4-nitrophenol (4-NP, Sigma Chemical Co., St. Louis, Mo., USA), the absorbance was observed at 400 nm by using a UV–Vis Spectrophotometer (UV-1601, Shimadzu, Japan).

2.2 Synthesis of Mag–SiO_2 and AuNP@Mag–SiO_2 Microspheres

Monodisperse-porous poly(MAA-co-EDMA) microspheres were prepared by a multi-step microsuspension polymerization developed in our previous study [30, 53, 54]. Polymeric microspheres used as template for the synthesis of magnetic silica microspheres were synthesized according to multistage microsuspension polymerization as described elsewhere [55]. Typically, $FeCl_3{\cdot}6H_2O$ (0.8 g) and $FeCl_2{\cdot}4H_2O$ (0.54 g) were mixed in 20 mL of distilled

water at ice bath. Then, the solution was poured into a flask containing the aqueous dispersion of poly(MAA-co-EDMA) microspheres and stirred at ice bath for 30 min under nitrogen blanket. The solution was then evacuated in vacuum and heated to 85 °C under mechanic stirring. Ammonium hydroxide solution (25 mL) was then added into the above solution mechanically stirred at 85 °C for 1 h. After being cooled, magnetic poly(MAA-co-EDMA) microspheres were magnetically separated, and followed by washing with deionized water several times.

The magnetic silica microspheres (Mag–SiO_2) were fabricated by a staged-shape template hydrolysis and condensation protocol by using magnetic poly(MAA-co-EDMA) microspheres as template synthesized with different Fe(III)/Fe(II) molar ratios [56]. Typically, magnetic poly(MAA-co-EDMA) microspheres (0.4 g) were dispersed in a solution containing 50 mL of Iso-PrOH and 5 mL of water. TBAI (0.25 g) and NH_4OH (0.25 mL, %25 w/w) were added into the mixture and sonicated for 5 min. The mixture was kept under mechanical stirring for 1 h and 5 mL of TEOS/Iso-PrOH solution (25/75 v/v) was added slowly into the mixture. The final medium was stirred for 20 h at 30 °C. The silica/polymer composite microspheres obtained were washed with Iso-PrOH and water and then dried at 80 °C for 12 h. Finally, monodisperse-porous magnetic silica microspheres were obtained after being calcinated at 450 °C for 3.5 h at a heating rate of 2 °C/min.

Fig. S1 in Supporting Information shows the procedure for the synthesis of AuNP@Mag–SiO_2 microspheres. Mag–SiO_2 microspheres (0.4 g) were modified by 3-aminopropyl triethoxysilane (APTES) (3 mL) within Iso-PrOH (20 mL). The resulting amine-functionalized magnetic silica microspheres were washed repeatedly with Iso-PrOH and water and then dried at 80 °C. Gold nanoparticles were prepared according to Martin method [57]. The flask containing an aqueous solution of $HAuCl_4$ (5.0×10^{-3} M in the same molar amount of HCl, 24 µL) was mixed with an aqueous stock solution of $NaBH_4$ (5.0×10^{-3} M in the same molar amount of NaOH, 100 µL) followed by adding a total volume of 10 mL distilled water. The light yellow solution turned to an orange color and then red in < 1 min. Amine-functionalized magnetic silica microspheres (0.02 g) were put into the mixture solution and the solution was stirred at room temperature for 6 h to obtain AuNP@Mag–SiO_2 microspheres.

2.3 Characterization

The median pore size, pore size distribution and the specific surface area of Mag–SiO_2 and AuNP@Mag–SiO_2 microspheres were determined by using Surface area and pore size analyzer system (Quantochrome, Nova 2200e, U.S.A.). The size and morphology of Mag–SiO_2 and AuNP@Mag–SiO_2 microspheres were investigated by Scanning Electron Microscopy (SEM, FEI,Quanta 200 FEG, U.S.A.). X-ray photoelectron spectroscopy (Thermo Scientific™ K-Alpha™ XPS spectrometer, MA, U.S.A.) was used to determine the surface composition. Magnetic measurements of Mag–SiO_2 and AuNP@Mag–SiO_2 microspheres were performed using a vibrating sample magnetometer (VSM, Quantum Design) at room temperature. X-ray diffraction spectrophotometer (XRD, Ultima IV X-ray diffractometer, Rigaku Ultima IV, Tokyo, Japan) measurements were performed to determine the crystal structures of Mag–SiO_2 and AuNP@Mag–SiO_2 microspheres.

2.4 Catalytic Activity of AuNP@Mag–SiO_2 Microspheres

The catalytic reduction of 4-NP to 4-AP was performed to evaluate the catalytic activity of AuNP@Mag–SiO_2 microspheres. The reaction was carried out at room temperature by monitoring the UV–vis spectra at 1 min intervals. Firstly 4-nitrophenol (0.027 g) was dissolved in 10 mL of distilled water. 4-NP solutions of certain concentration was prepared by diluting from stock solution. $NaBH_4$ (0.2 g) was added to the solution. After adding the catalyst developed to the 4-NP solution, the degradation rate was observed by reading the spectra at a wavelength of 400 nm as a function of time in the presence of excess amount of $NaBH_4$.

The catalytic reduction of 4-NP as a function of reaction time (Eq. (1)) is given by:The catalytic reduction of 4-NP:

$$\left([4-\mathrm{NP}]_0 - [4-\mathrm{NP}]_t\right)/[4-\mathrm{NP}]_0 \times 100 \quad (1)$$

where $[4NP]_0$ is the concentration of 4NP at the initial time of the reaction, and $[4\text{-NP}]_t$ is the concentration of 4NP at time t.

It is thought that the concentration of $NaBH_4$ remains constant during the reaction in the presence of an excess of $NaBH_4$ compared to 4-NP. Therefore pseudo first-order kinetics was used with respect to 4-NP to determine the catalytic rate of the reaction. The rate constant, k (min^{-1}) can be calculated by using Eq. (2):

$$\mathrm{In}\left(C_t/C_o\right) = \mathrm{In}\left(A_t/A_o\right) = -k \times t \quad (2)$$

k is the pseudo-first-order kinetic rate constant and is calculated by a linear fitting. C_t is the concentration of 4-nitrophenol during the reaction at any time and C_0 is the initial concentration of 4-nitrophenol. A_t is the maximal absorbance of 4-NP at any time and A_0 is the initial absorbance of 4-NP.

3 Results and Discussion

The monodisperse porous polymer microspheres were obtained by multi-stage microsuspension polymerization to be used as the template material for the synthesis of magnetic silica microspheres. In the presence of Fe^{2+} and Fe^{3+} salts, the magnetic microspheres were obtained by using binary precipitation protocol [55, 56]. Monodisperse porous Mag–SiO_2 microspheres were obtained by calcination of silica-polymer composite in an oven at 450 °C for 3.5 h. Mag–SiO_2 microspheres were modified by APTES because of the increased interaction with AuNP through coordinated bonds, resulting in effective deposition of AuNP on silica support.

The SEM photographs showing the surface morphology, the average size and size distribution for Mag–SiO_2 and AuNP@Mag–SiO_2 microspheres are given in Fig. 1. The pore size distribution curves of magnetic silica microspheres synthesized with different Fe(III)/Fe(II) molar ratios and AuNP@Mag–SiO_2 microspheres are given in Fig. S2 in Supporting Information. The porous properties calculated based on the pore size distribution curves, size and the saturation magnetization values of synthesized magnetic microspheres are included in Table 1. As seen in Fig. 1 and Table 1, the obtained microspheres are uniform with a mean diameter of 6.20–6.80 µm with the coefficient of variation was 4.0–5.5%. The photographs also demonstrate the presence of both the meso and the macroporous structure of the silica microspheres. These pores provided immobilization of the gold nanoparticles on the porous surface. Although the highest saturation magnetization (i.e. 50 emu/g) was obtained with Fe(III)/Fe(II) molar ratio of 2.2, the pore volume and the specific surface area of this sample were considerably lower with respect to the other formulations. On the other hand, the saturation magnetizations and the specific surface areas of magnetic microspheres obtained with Fe(III)/Fe(II) molar ratios of 0.5 and 1.1 were very close (Table 1). By considering its higher porosity (i.e. higher pore volume), magnetic silica microsphere sample obtained with Fe(III)/Fe(II) molar ratio of 1.1 was chosen as the appropriate support for the attachment of Au nanoparticles.

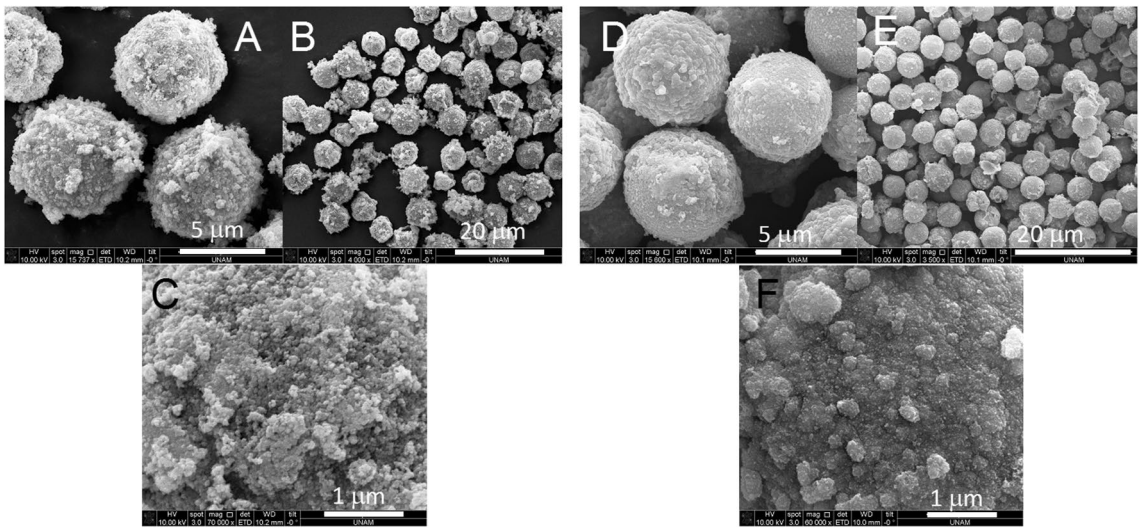

Fig. 1 SEM photographs of (**a**–**c**) Mag–SiO_2 and (**d**–**f**) AuNP@Mag–SiO_2 microspheres, Magnification: **a**, **d** ~ × 4000, **b**, **e** ~ × 15,000, **c**, **f** ~ × 70,000

Table 1 The size and porous properties of Mag–SiO_2 synthesized with different Fe(III)/Fe(II) molar ratios and AuNP@Mag–SiO_2 microspheres

Microspheres	Fe(III)/Fe(II) molar ratios	D_n (µm)	CV (%)	D_m (nm)	V_p (cc/g)	SSA (m^2/g)	M (emu/g)
Mag–SiO_2	1.1	6.20	5.2	38.92	0.40	194.87	33.6
Mag–SiO_2-1	0.5	6.28	4.02	40.30	0.30	205.70	36.0
Mag–SiO_2-2	2.2	6.80	4.95	52.60	0.12	86.61	50.0
AuNP@Mag–SiO_2	1.1	6.23	5.5	42.71	0.38	90.40	29.3

D_n Average particle size, *CV* coefficient of variation for size distribution, *SSA* specific surface area, *Vp* Pore volume, D_m Median pore size, *M* saturation magnetization

As revealed by the pore size distribution curves given in Fig. S2 in Supporting Information, the surface area and the pore volume decreased as a result of loading of AuNP into the porous silica matrix. The concentration of AuNP on the surface of Mag-SiO_2 microspheres was determined as 2.09% w/w by XPS spectrometer (Table S1 in Supporting Information).

The microspheres must have sufficient saturation magnetization to perform a facile and efficient removal from the reaction medium by the application of an external magnetic field. Saturation magnetization values measured at room temperature were found to be 33.6 and 29.3 emu g^{-1} for Mag–SiO_2 and AuNP@Mag–SiO_2 microspheres, respectively (Fig. S3A in Supporting Information). The decrease in the magnetic saturation is a result of the deposition of AuNP into silica matrix. The trials showed that the AuNP@Mag–SiO_2 microspheres could be separated from the reaction medium by the use of an external magnet within the time-periods less than 1 min. XRD measurement result of AuNP@Mag–SiO_2 microspheres is given in Fig. S3B in Supporting Information. XRD diffraction peaks were observed at 2θ values of 30.10°, 35.54°, 43.09°, 53.46°, 56.98°, and 62.58° due to the magnetic iron oxide content of the microspheres. The four characteristic peaks at 2θ values of 38.18°, 44.39°, 64.58°, and 77.55° obtained for AuNP@Mag–SiO_2 microspheres confirm the presence of Au loaded into the microstructure.

3.1 Catalytic Reduction of 4-NP

The catalytic activity of AuNP@Mag–SiO_2 microspheres was tested in the reduction of 4-NP to 4-aminophenol (4-AP). In the reaction, while the 4-NP solution gave the characteristic absorbance peak at 320 nm, it was shifted to 400 nm due to the 4-nitrophenolate ions formed by the addition of $NaBH_4$ to the solution. After adding AuNP@Mag–SiO_2 microspheres to the reaction, the peak at 400 nm decreases with time, resulting in the formation of 4-AP at 300 nm, which increases gradually with time (Fig. 2a). Gold nanoparticles as a plasmonic catalyst acts as an electronic relay system to overcome the kinetic barrier caused by the large potential difference between 4-nitrophenolate and $BH4^-$ ions. Thus AuNP have the ability to catalyze the formation of 4-aminophenol [58]. The Langmuir–Hinshelwood (LH) mechanism of reduction of 4-NP to 4-AP in the presence of excess amount of $NaBH_4$ using the AuNP@Mag–SiO_2 microparticles is shown in Fig. 2b.

In the mechanism, the borohydride ions are adsorbed onto the catalyst surface, transferring hydrogen to the catalyst surface. At the same time, 4-NP is adsorbed onto the catalyst surface. 4-NP reacts with the hydrogen atoms on the surface to form the 4-AP product. After desorbing 4-AP product from the surface, the catalyst can be separated and reused due to its magnetic properties.

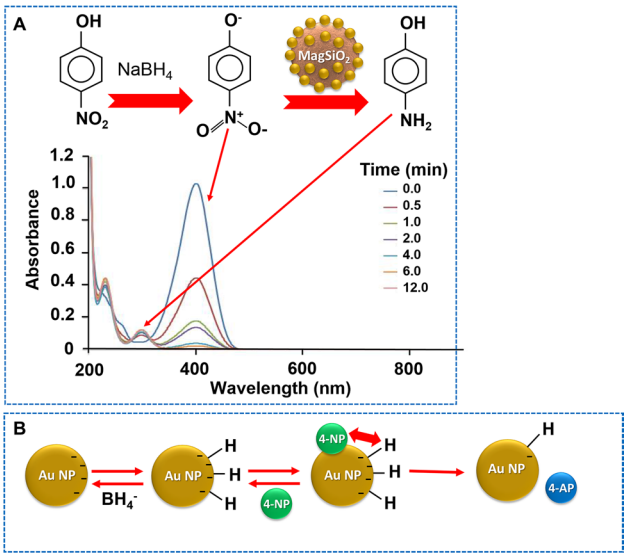

Fig. 2 **a** UV–Vis absorption spectra obtained during the catalytic chemical reduction of 4-NP. **b** Langmuir–Hinshelwood mechanism of the reduction of 4-NP by using AuNP@Mag–SiO_2 microspheres in the presence of $NaBH_4$

3.1.1 Effect of Temperature on Reduction

The variation of 4-NP concentration with the reaction temperature is given in the Fig. S4A in Supporting Information. The results given in the Fig. S4 in Supporting Information show that the conversion of 4-NP at 40 °C is significantly faster. It is also seen that almost complete conversion of 4-NP is achieved with reasonably short reaction periods at all temperatures, by using AuNP@Mag-SiO_2 microspheres. The rate constants are calculated for the degradation of 4-NP between 10 and 40 °C (Fig. S4B in Supporting Information). As expected the rate constant increases with the increase in temperature as the probability of collision frequency of molecules increases at higher temperatures.

3.1.2 Effect of Amount of Catalyst on Reduction

The effect of the catalyst amount on the reaction rate was investigated in the 4-NP degradation performed at room temperature. As shown in the Fig. 3, when the amount of catalyst is too low (0.5 mg) the reaction period becomes so long (30 min). At a high catalyst amount (4 mg), almost 99% of 4-NP degradation is completed in a short period such as 4 min. As seen in Fig. 3b, the reaction rate linearly increases with increasing catalyst amount as also shown by different researchers [5, 59].

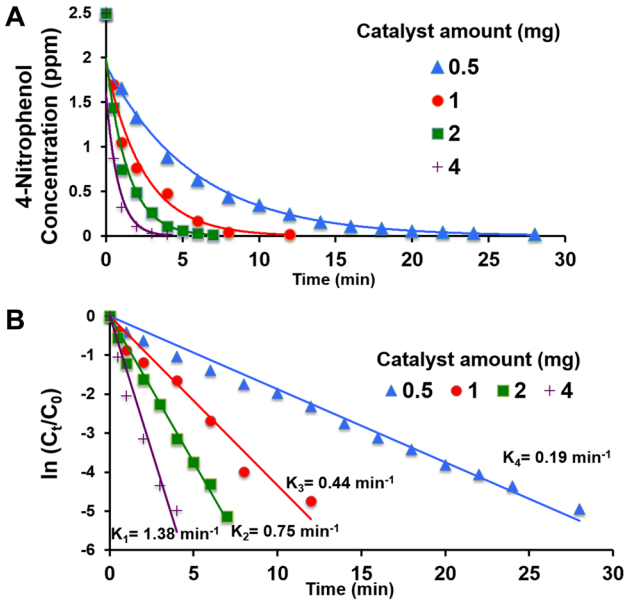

Fig. 3 **a** The variation of 4-NP concentration (ppm) with the time using AuNP@Mag–SiO_2 microspheres as catalyst, **b** Plot of $\ln(C_t/C_0)$ versus time for the reduction of 4-NP with different catalyst amount (the kinetic rate constans (min^{-1}) are shown on the graph). Reaction conditions: Au loading (w/w%): 5%; Catalyst amount: 0.5, 1, 2, 4 mg; 4-NP concentration: 2.5 ppm, and reaction temperatures of 20 °C

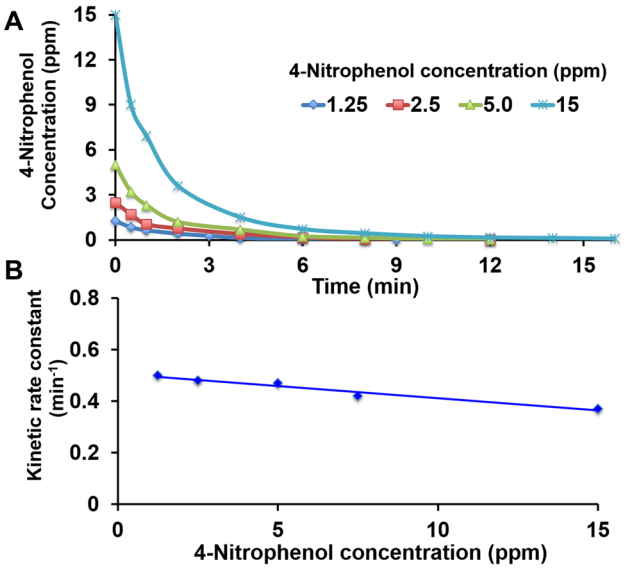

Fig. 4 **a** The variation of 4-NP concentration (ppm) with the time using AuNP@Mag–SiO_2 microspheres as catalyst with different 4-NP concentration. **b** Plot of the kinetic rate constants (min^{-1}) versus 4-NP concentration (ppm). Reaction conditions: Au loading (w/w%): 5%; Catalyst amount: 1 mg; 4-NP concentration (ppm): 1.25, 2.5, 5.0, 15, and reaction temperatures of 20 °C

3.1.3 Effect of Initial 4-NP Concentration on Reduction

The effect of the initial 4-NP concentration on the reaction rate was investigated by changing initial phenol concentration between 1.25 and 15 ppm. When 1.25 ppm phenol concentration was used, the degradation process was completed in a short time such as 5 min, while the time of degradation increased for other 4-NP concentrations (Fig. 4a). These studies confirm that the rate of reduction of 4-nitrophenol decreases with the increasing initial 4-nitrophenol concentration probably due to the limiting number of active sites on the AuNP@Mag–SiO_2 catalyst (Fig. 4b).

3.1.4 Effect of Au Loading on Reduction

In a typical catalytic reaction, these steps (1) adsorption of the reactant to the catalyst surface, (2) diffusion of the reactant into the pores (3) reaction from the reactant to the product (4) desorption of the product, are carried out. The rate of reaction is directly proportional to the catalytic activity of Au, which is most dependent on the amount of Au loading. As seen in the Fig. S5 in Supporting Information, the reaction rate decreases and reaction time increases with the increasing Au loading probably due to the increased aggregation of AuNP on the porous silica support.

3.2 Comparision of Catalytic Activities

The catalytic activity of the developed plasmonic catalyst was compared to the activities of other plasmonic catalysts developed for the degradation of 4-NP in the literature (Table 2). For the correct evaluation of the catalytic performance, k/m (the reaction rate constant per the Au content of the used catalysts) was used as the activity parameter. The results showed that the developed catalyst had a competitiveness with other catalysts used in the literature [40, 60–63]. In addition, the magnetic properties of the catalyst and the use of silica as a support material have enabled the catalyst to have superior properties than some catalysts used in the literature [40, 60–63].

Table 2 Comparison of pseudo-first-order rate constant for nitrophenol reduction by using Au based catalysts

Catalyst	k (min^{-1})	k ($min^{-1}g^{-1}$)	Ref.
Fe_30_4@SiO_2–Au@m SiO_2	0.35	5830	40
Au–Fe_30_4	0.63	1657	61
Au@SiO_2	0.234	720	62
TiO_2@GOS@Au	0.90	3214	63
Au/TiO_2 hybrid nano fibers	0.244	244	64
AuNP@Mag–SiO_2 microspheres	1.380	6900	This work

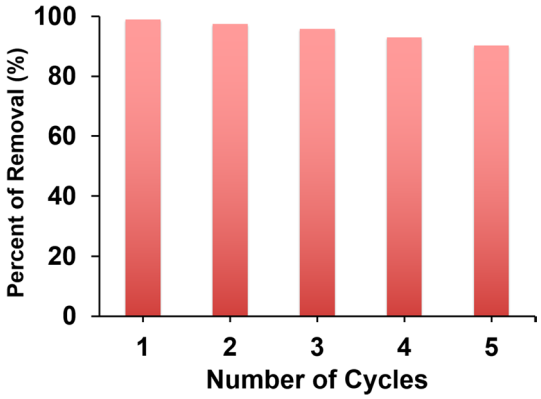

Fig. 5 Reusability of AuNP@Mag–SiO_2 microspheres for reduction of 4-NP. (Calcination temperature: 450 °C, temperature: 20 °C, catalyst amount: 1 mg, 4-NP concentration: 2.5 ppm, Au loading (w/w%): 5%)

The catalyst was prepared using monodisperse-porous silica spheres in micron-size range as the base material. The saturation magnetization of magnetic silica microspheres was determined as 33.6 emu/g. With respect to the commonly used magnetic nanoparticles, the selection of a micron-size support with satisfactorily high saturation magnetization allowed fast separation of synthesized catalyst from the reaction medium. As seen in Fig. S3 of Supporting Information, the catalyst could be completely removed from the reaction medium by using an external magnet within 2–3 s. On the other hand, the selection of porous support with high specific surface area allowed the deposition of high number of AuNP onto per mass of base material (i.e. porous silica microspheres). Extremely higher reaction rate constants achieved with respect to similar catalysts in Table 2 should be likely explained by this property of the synthesized catalyst.

3.3 Recyclability and Stability

The stability and reproducibility of the catalyst developed is an important parameter. For this purpose, the catalyst was separated from the reaction mixture by using external magnet and used again in 4-NP degradation under the same reaction conditions. The results showed that the catalyst could be repeatedly reused with high conversion (> 90) over five runs (Fig. 5).

4 Conclusion

The plasmonic catalytic activity of AuNP@Mag–SiO_2 microspheres in the reduction of 4-NP was investigated by changing Au loading, reaction temperature, amount of catalyst and initial concentration of 4-NP. AuNP@Mag–SiO_2 microspheres demonstrated high catalytic activity with good repeatability and magnetic separation ability. The use of magnetic porous SiO_2 microspheres as support material provided high surface area, large pore volume and efficient mass transfer. The kinetics of degradation of 4-NP was pseudo-first-order and the degradation was completed within the reaction periods < 4 min in the catalytic runs performed by using AuNP@Mag–SiO_2 microspheres as a plasmonic catalyst. AuNP@Mag–SiO_2 microspheres are promising as a new Au-based catalyst for the degradation of 4-NP.

On the other hand, when the core–shell $BaTiO_3$@SiO_2 nanostructures and Fe_3O_4/silica/Fe_3O_4 nanoparticles previously developed are considered, AuNP@Mag-SiO_2 microspheres can be evaluated as the promising materials which is potentially capable of providing a high insulating SiO_2 layer and a large interface for high polarization particularly for energy storage applications [64, 65].

Acknowledgements This research is supported by Hacettepe University Scientific Research Projects Coordination Unit under contract numbered as FHD-2015-6266. The author acknowledges use of the services and facilities of UNAM-National Nanotechnology Research Center at Bilkent University. The author thank Prof.Dr. Ali TUNCEL for his valuable help to use his own laboratory facilities.

References

1. Y. Liu, Y. Chen, Y.Y. Zhang, Q.W. Kou, Y.X. Wang, L. Chen, Y.T. Sun, H.L. Zhang, Y.M. Jung, Molecules **23**, 1330 (2018)
2. Y.M. Liu, H. Tsunoyama, T. Akita, S.H. Xie, T. Tsukuda, ACS Catal. **1**, 2 (2011)
3. S. Wang, L.P. Xu, X. Zhang, Sci. Adv. Mater. **7**, 2084 (2015)
4. Y. Liu, Y.Y. Zhang, Q.W. Kou, Y. Chen, Y.T. Sun, D.L. Han, D.D. Wang, Z.Y. Lu, L. Chen, J.H. Yang, S.G. Xing, Nanomaterials **8**, 329 (2018)
5. S. Panigrahi, S. Basu, S. Praharaj, S. Pande, S. Jana, A. Pal, S.K. Ghosh, T. Pal, J. Phys. Chem. C **111**, 4596 (2007)
6. Z.Y. Ji, X.P. Shen, G.X. Zhu, H. Zhou, A.H. Yuan, J. Mater. Chem. **22**, 3471 (2012)
7. Y. Chen, Y.Y. Zhang, Q.W. Kou, Y. Liu, D.L. Han, D.D. Wang, Y.T. Sun, Y.J. Zhang, Y.X. Wang, Z.Y. Lu, S.G. Xing, Nanomaterials **8**, 353 (2018)
8. S.J. Hoseini, M. Rashidi, M. Bahrami, J. Mater. Chem. **21**, 16170 (2011)
9. X. Li, L. Xing, K. Zheng, P. Wei, L. Du, M. Shen, X. Shi, ACS Appl. Mater. Interfaces **9**, 5817 (2017)
10. C. Wu, D. Li, L. Wang, X. Guan, Y. Tian, H. Yang, S. Li, Y. Liu, Acta Biomater. **53**, 631 (2017)
11. J. Wang, X. Wu, C. Wang, Z. Rong, H. Ding, H. Li, S. Li, N. Shao, P. Dong, R. Xiao, S. Wang, ACS Appl. Mater. Interfaces **8**, 19958 (2016)
12. U. Aslam, S. Chavez, S. Linic, Nat. Nanotechnol. **12**, 1000 (2017)
13. S.T. Hunt, M. Milina, A.C. Alba-Rubio, C.H. Hendon, J.A. Dumesic, Y. Román-Leshkov, Science **352**, 974 (2016)

14. S.M. El-Sheikh, A.A. Ismail, J.F. Al-Sharab, N. J. Chem. **37**, 2399 (2013)
15. J.R. Chiou, B.H. Lai, K.C. Hsu, D.H. Chen, J. Hazard. Mater. **248**, 394 (2013)
16. Q. Zhang, H. Wang, ACS Catal. **4**, 4027 (2014)
17. J.M. Zhang, G.Z. Chen, M. Chaker, F. Rosei, D.L. Ma, Appl. Catal. B: Environ. **132**, 107 (2013)
18. L.H. Qiu, Y.J. Peng, B.Q. Liu, B.C. Lin, Y. Peng, M.J. Malik, Y. Yan, Appl. Catal. A **413**, 230 (2012)
19. J. Zeng, Q. Zhang, J.Y. Chen, Y.N. Xia, Nano Lett. **10**, 30 (2010)
20. H.B. Chong, P. Li, J. Xiang, F.Y. Fu, D.D. Zhang, X.R. Ran, M.Z. Zhu, Nanoscale **5**, 7622 (2013)
21. S.N. Wang, M.C. Zhang, W.Q. Zhang, ACS Catal. **1**, 207 (2011)
22. A. Gangula, R. Podila, M. Ramakrishna, L. Karanam, C. Janardhana, A.M. Rao, Langmuir **27**, 15268 (2011)
23. A.S.K. Hashmi, G.J. Hutchings, Angew. Chem. Int. Ed. **45**, 7896 (2006)
24. C.W. Corti, R.J. Holliday, D.T. Thompson, Appl. Catal. A: Gen. **291**, 253 (2005)
25. Y. Mikami, A. Dhakshinamoorthy, M. Alvaro, H. García, Catal. Sci. Technol. **3**, 58 (2013)
26. X. Chen, H.Y. Zhu, J.C. Zhao, Z.T. Zheng, X.P. Gao, Angew. Chem. Int. Ed. **47**, 5353 (2008)
27. R.J. White, R. Luque, V.L. Budarin, J.H. Clark, D.J. Macquarrie, Chem. Soc. Rev. **38**, 481 (2009)
28. Y. Li, Y. Pan, L. Zhu, Z. Wang, D. Su, G. Xue, Macromol. Rapid Commun. **232**, 1741 (2011)
29. G.B.B. Varadwaj, K.M. Parida, RSC Adv. **3**, 13583 (2013)
30. G. Gunal, C. Kip, E. Ogut, D.D. Usta, E. Senlik, G. Kibar, A. Tuncel, Mater. Sci. Eng. C Mater. Biol. Appl. **74**, 10 (2017)
31. C. Kip, H. Gülüşür, E. Çelik, D.D. Usta, A. Tuncel, Colloids Surf. B **174**, 333 (2019)
32. X. Li, L. Zhao, C. Shao, X. Li, W. Sun, Y. Liu, J. Colloid Interface Sci. **530**, 345 (2018)
33. A.M. Khalil, V. Georgiadou, M. Guerrouache, S. Mahouche-Chergui, C. Dendrinou-Samara, M.M. Chehimi, B. Carbonnier, Polymer **77**, 218 (2015)
34. N. Muthuchamy, A. Gopalan, K.P. Lee, RSC Adv. **5**, 76170 (2015)
35. Z. Sun, H. Li, G. Cui, Y. Tian, S. Yan, Appl. Surf. Sci. **360**, 252 (2016)
36. M. Rocha, C. Fernandes, C. Pereira, S.L.H. Rebelo, M.F.R. Pereira, C. Freire, RSC Adv. **5**, 5131 (2015)
37. F. Bibi, M. Ajmal, F. Naseer, Z.H. Farooqi, M. Siddiq, Int. J. Environ. Sci. Technol. **15**, 863 (2017)
38. N. Pradhan, A. Pal, T. Pal, Colloids Surf. A **196**, 247 (2002)
39. K. Esumi, K. Miyamoto, T. Yoshimura, J. Colloid Interface Sci. **254**, 402 (2002)
40. Y.H. Deng, Y. Cai, Z.K. Sun, J. Liu, C. Liu, J. Wei, W. Li, C. Liu, Y. Wang, D.Y. Zhao, J. Am. Chem. Soc. **132**, 8466 (2010)
41. Y. Zhu, J. Shen, K. Zhou, C. Chen, X. Yang, C. Li, J. Phys. Chem. C **115**, 1614 (2011)
42. Z. Zhang, C. Shao, P. Zou, P. Zhang, M. Zhang, J. Mu, Z. Guo, X. Li, C. Wang, Y. Liu, Chem. Commun. **47**, 3906 (2011)
43. P. Liu, M.F. Zhao, Appl. Surf. Sci. **255**, 3989 (2009)
44. H. Shang, L. Du, H. Guan, B. Zhang, X. Xiang, ChemistrySelect **3**, 5066 (2018)
45. H. Guan, C. Chao, Y. Lu, H. Shang, Y. Zhao, S. Yuan, B. Zhang, J. Chem. Sci. **128**, 1355 (2016)
46. H. Shang, K. Pan, L. Zhang, B. Zhang, X. Xiang, Nanomaterials **6**, 103 (2016)
47. H. Liu, C. Lin, Z. Ma, H. Yu, S. Zhou, Molecules **18**, 14258 (2013)
48. Y. Li, C. Jin, G. Yuan, J. Han, M. Wang, R. Guo, Langmuir **33**, 7486 (2017)
49. Z. Wang, H. Fu, D. Han, F. Gu, J. Mater. Chem. A **2**, 20374 (2014)
50. Z. Dong, G. Yu, X. Le, New J. Chem. **39**, 8623 (2015)
51. F. Zhang, P. Yang, K. Matras-Postolek, J. Nanosci. Nanotechnol. **16**, 5966 (2016)
52. S. Zhou, X. Yao, T. Fan, RSC Adv. **6**, 102258 (2016)
53. T. Camli, M. Tuncel, S. Senel, A. Tuncel, J. Appl. Polym. Sci. **84**, 414 (2002)
54. C. Kip, R.B. Tosun, S. Alpaslan, I. Kocer, E. Celik, A. Tuncel, Talanta **200**, 100 (2019)
55. K. Salimi, D.D. Usta, Ö. Çelikbıçak, A. Pinar, B. Salih, A. Tuncel, Colloids Surf. B Biointerfaces **153**, 280 (2017)
56. K. Salimi, D.D. Usta, I. Kocer, E. Celik, A. Tuncel, RSC Adv. **7**, 8718 (2017)
57. M.N. Martin, J.I. Basham, P. Chando, S.K. Eah, Langmuir **26**, 7410 (2010)
58. S.K. Ghosh, M. Mandal, S. Kundu, S. Nath, T. Pal, Appl. Catal. A **268**, 61 (2004)
59. Y. Li, J.Y. Lan, J. Liu, J. Yu, Z. Luo, W. Wang, L. Sun, Ind. Eng. Chem. Res. **54**, 5656 (2015)
60. F. Lin, R. Doong, J. Phys. Chem. C **115**, 6591 (2011)
61. J. Lee, J.C. Park, H. Song, Adv. Mater. **20**, 1523 (2008)
62. H. Kang, M. Kim, K.H. Park, Appl. Catal. A **502**, 239 (2015)
63. Y. Hao, X. Shao, B. Li, L. Hu, T. Wang, Mater. Sci. Semicond. Process. **40**, 621 (2015)
64. K. Bi, M. Bi, Y. Hao, W. Luo, Z. Cai, X. Wang, Y. Huang, Nano Energy **51**, 513 (2018)
65. H. Hu, H. Liu, D. Zhang, J. Wang, G. Qin, X. Zhang, Eng. Sci. **2**, 43 (2018)